Desalination and Water Treatment
www.deswater.com
doi: 10.1080/19443994.2015.1084592

57 (2016) 17384–17399
August

Taylor & Francis
Taylor & Francis Group

Characterization of different types of bentonites and their applications as adsorbents of Co(II) and Ni(II)

Majid Hayati-Ashtiani[a,*], Hadi Azimi[b]

[a]*Faculty of Engineering, Department of Chemical Engineering, University of Kashan, P.O.Box: 873175-1167, Kashan, Iran, Tel. +98 31 55912424; email: hayati@kashanu.ac.ir*
[b]*Faculty of Letters and Human Sciences, Department of English, Shahid Beheshti University, P.O.Box: 198396-3113, Tehran, Iran, Tel. +98 21 73932324; email: ha_azimi@sbu.ac.ir*

Received 1 August 2014; Accepted 15 August 2015

ABSTRACT

In this research, the natural bentonite clays collected from different areas in Iran were utilized as adsorbent to study the removal behavior of different Iranian bentonitic clays vs. Ni(II) and Co(II) from their aqueous solutions. The original bentonite clays were characterized with the help of pH, Swell Index, Sediment Index, granulometric (screen) analysis, cation exchange capacity measurement, powder X-ray diffraction, X-ray fluorescence, scanning electron microscopy with energy dispersive atomic X-ray; Brunauer, Emmett, and Teller surface area measurements; and Barrett, Joyner, and Halenda pore size distribution analysis, Fourier transform infrared spectroscopy. While the thermal stability of the samples was studied using thermo gravimetry (TGA-DSC), adsorption experiments were conducted under some constant solution conditions and the removal of Co^{2+} and Ni^{2+} ions from their aqueous solutions was tested on various bentonite types and certain bentonite characteristics including pore size, surface properties, etc. The maximum adsorption of 92% took place on sample *A*1 in the removal process of Co^{2+} and Ni^{2+}. The adsorption capacities followed the order of $Co^{2+} > Ni^{2+}$ in single-component systems for sample *A*2 and *A*3. The results showed the prevailing metal removal process was adsorption and cation exchange with the initiation in precipitation.

Keywords: Adsorption; Bentonite; Co(II) and Ni(II); Nano-porous Montmorillonite; Cation Exchange

1. Introduction

The presence of heavy metals in industrial effluents is currently a serious global environmental problem. Cobalt and nickel are highly toxic elements endangering the environment. They are the 27 and 28 members of the Mendeleyev periodic table, respectively. Co(II) and Ni(II) may have similar physio-chemical properties since they have the closest molecular weight, i.e. 125.3 and 124.6 g mol, respectively.

Co(II) is widely used in research and medical applications [1–4], and the liquid wastes are released from pressurized water from the nuclear power reactors [3,5], whereas Ni(II) is one of the most widely utilized elements in different industries such as manufacturing process of stainless steel, super alloys,

*Corresponding author.

metallic alloys, electroplating industry, minting currency coins, processing different materials for the production of paints and mass production of different types of batteries. Some groundwater resources are contaminated by leachate from landfills where used batteries are discharged [6–9]. High doses of Co(II) can cause different serious diseases such as paralysis, diarrhea, low blood pressure, lung irritations, and bone defects [10]. Ni(II) is an essential nutrient needed by the body in trace amounts. However, an increase in the chronic exposure of humans to high Ni(II) concentrations may cause fatal diseases such as lung, nose and bone cancers [7], birth defects, embolism, chronic bronchitis [11], and dermatitis [6].

Various methods for heavy metal removal including Co(II) and Ni(II) cations from solutions have already been developed. The most widely used methods still in use are chemical precipitation, reverse osmosis (RO), ion exchange, solvent extraction, coagulation–flocculation, evaporation, electro flotation, electrodialysis, membrane separation, electro deposition, chelation, biosorption, and adsorption [6,10–16]. Furthermore, some other technologies such as ultrafiltration combined with complexation [17,18], electro coagulation [19], RO alone and combined with lime precipitation [20], electroflotation [21], photocatalytic treatment [22], and nano-filtration [23] have also been tested for the removal of Ni(II). Obviously, each of the treatment technologies being used today has its own advantages and disadvantages. Among all these methods, adsorption appears to be an economical and feasible alternative method for the removal of heavy metals from wastewater [24]. Several adsorbents including chitosan [25], yeast [26,27], lignin [28], montmorillonite (bentonite) [29], compost [30], iron-based sorbents [31], activated carbon, sludge [32], and specific type of micro-organisms [33–35] have been employed for Co(II) and Ni(II) removal. The costs of some of the important commercial adsorbents are listed in Table 1 [36].

Bentonite presents a promising mineral which has been successfully applied for the removal of heavy metals from wastewater. Due to its high adsorption and cation exchange ability, montmorillonite minerals are able to effectively remove cations from solutions.

Table 1
Cost comparison of clays (including montmorillonite) with common adsorbents

Types of adsorbent	Price (US $ kg^{-1})
Clays (including montmorillonite)	0.04–0.12
Commercial activated carbon (CAC)	20–22.00
Chitosan	15.43

Clays containing montmorillonite (Fig. 1) are referred to as bentonite, which belongs to the 2:1 phyllosilicate clay minerals. The reason of deficiency in the positive charge of montmorillonite is due to the isomorphic substitution of Al for Si in the tetrahedral sheets and Mg for Al in the octahedral sheets of the 2:1 layers of montmorillonite. The negative structural electric charge (commonly, 0.66 charges per unit cell) is balanced by the cations located between the unit layers of the montmorillonite dioctahedral structure. These cations are thus dissolved into the aqueous solution (leaving the surface negatively charged) and/or exchanged for other cations from the solution. There is also a positive pH-dependent charge at the edges of the lamellar particles, but it is too small to overcome the negative charge on the lamellar faces [37,38].

In this study, bentonites are categorized into three types, namely swelling (Na-montmorillonite), non-swelling–swelling (Ca, Na-montmorillonite), and non-swelling (Ca-montmorillonite). Bentonites especially the sodic (swelling) type can adsorb huge amount of water compared to its dry weight. Such process is accompanied by swelling allowing the intimate contact of the clay particles with other compounds. Swelling of bentonite is mainly caused by the swelling of montmorillonite [39], and this swelling is an important property of clay minerals. The presence of several layers of water molecules causes the basal spacing of smectites (montmorillonites) to increase from 1.05 nm or less to the order of 1.25–2.00 nm, depending on both the type of the clay and the exchangeable cations [40].

The literature contains few adsorption studies of Co(II) ions using bentonite. Manohar et al. [41] showed Al-pillared bentonite used in their study with the adsorption capacity of 38.61 mg g^{-1} was more effective for adsorption purposes than that of natural bentonite. Yu et al. [2,3] and Li et al. [42] studied the adsorption of Co(II) on bentonite in the presence and absence of fulvic acid under ambient conditions. Nagy et al. [43] studied Co(II) adsorption on montmorillonite and found that Co(II) adsorption increased from 10 to 100% at pH ranging from 2 to 7. They found the ion exchanges between Co and Ca-montmorillonite (or H) were the main mechanism of Co(II) uptake to montmorillonite. Bentonite and formaldehyde-modified bentonite (MF-bentonite) were tested for removal of the radioactive isotope ^{60}Co. Some enhancement obtained in the meso-pore region due to impregnating the bentonite with 35% of formaldehyde solution, and the modified sample had better adsorption

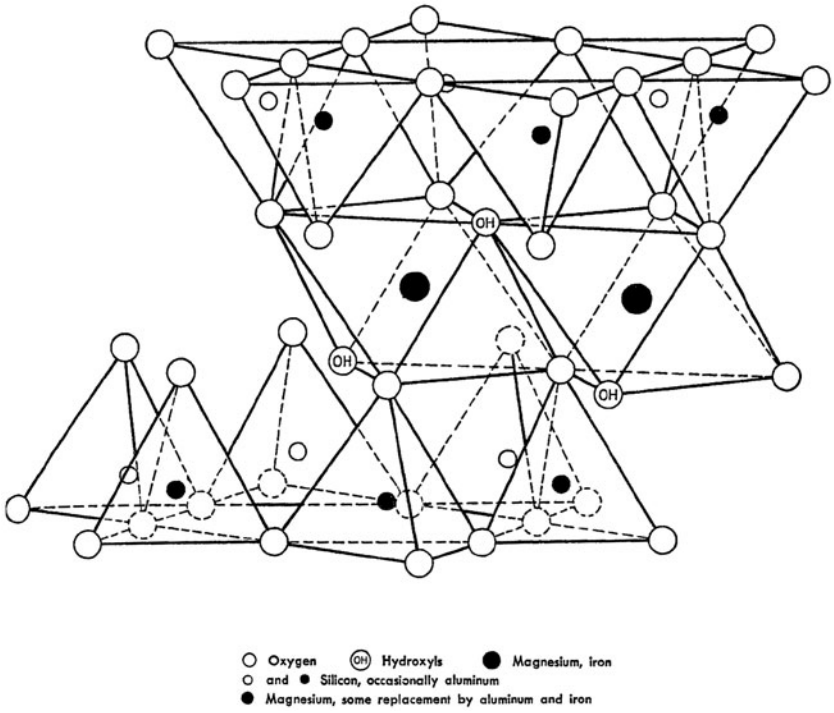

Fig. 1. Graphic sketch of the nano-montmorillonite.

performance [25] than that of natural bentonite. The composite adsorbent was tested for the removal of Co^{2+} ions in aqueous solution at various contact times, concentrations, pH, and repetitive loadings, and the new adsorbent showed effective removal after re-use and the adsorption increased with increasing initial pH [44]. Literature studies of Ni(II) removal showed [45] that Na-montmorillonite adsorbs Ni(II) even when organic substances (bonds) are presented. Abollino et al. [45] also studied the adsorption of Ni(II) onto Na- or swelling montmorillonite from wastewater in the presence of ligands, and they concluded that swelling montmorillonite is an effective sorbent for Ni removal. The removal of Ni(II) from aqueous solution on the Na-montmorillonite showed equilibrium for Ni(II) onto Na-montmorillonite was reached in 200 min, and the adsorption of Ni(II) was pH dependent in the pH range 2–9 [46]. In Covelo et al. [47], Ni was adsorbed in bentonite simultaneously from solutions with different concentrations. The adsorption of toxic metal Ni on natural and modified, pillared and acid activated montmorillonite was described by researchers [36]. Malamis et al. [48] described the adsorption properties of bentonites. Ijagbemi et al. [29] found that montmorillonite has a considerable potential for the removal of heavy metal cationic species, such as Ni(II) from aqueous solutions and wastewater. Álvarez-Ayuso and Garćia-Sánchez [49] utilized natural bentonite for the removal of Ni(II) from wastewater solutions of galvanic industries.

Although the results related to removal of Co(II) and Ni(II) on bentonite are significant and promising, a better understanding of the results is needed regarding adsorbent properties like swelling for the optimization of the separation process conditions. This study aims at investigating the effectiveness of bentonite in removing Ni(II) and Co(II) from aqueous solutions. Initially, the adsorbent was characterized in its natural conditions. Experiments were conducted to define the swelling and non-swelling properties of bentonites, especially Na-montmorillonite and Ca-montmorillonite types. Then, total Co(II) and Ni(II) removal percentage on clay was conducted according to swelling, nonswelling–swelling, and nonswelling bentonites.

2. Materials and methods

2.1. Materials and reagents

Clays that were used in this study were bentonites. Three bentonite samples, namely *A*1, *A*2, and *A*3, were used in their natural forms. The name, origin, and supplier of the bentonite samples are given in Table 2.

Table 2
Origin and supplier of bentonite samples

Sample name	Location of mine	Supplier
*A*1	Mehrijan, Isfahan Province of Iran	Kavir Bentonite Co., Isfahan Province of Iran
*A*2	Toroud, Semnan Province of Iran	Iran Mineral Processing Co., Seyed Abad Industrial Zone, Semnan, Iran
*A*3	Khoor-o Biabanak, Isfahan Province of Iran	Iran Barite Falat Co., Tehran Province of Iran

At the site, the air-dried chunks (<30 cm in diameter) were ground by primary and secondary (if necessary) jaw crushers (double toggle jaw crusher, type 1212, Aubema, Bergneustadt, Germany) to <5 cm. Then, less than 5 cm chunks were ground to 30–40 mm in diameter by a hammer crusher (impact hammer crusher, Aubema, Bergneustadt, Germany). At this stage, bentonites were sent into laboratory. At laboratory, samples were first dried using an oven (Fan Azma Gostar V.2.1, Iran) overnight, and then, the dried samples were further ground by laboratory jar and ball mill. Three prepared samples were powdered to less than 75 μm (US Standard Sieve Mesh No. 200, Pars Sieve, Iran) [ASTM E: 11] and used for analyses.

Analytical grade chemical (Merck) was used throughout the investigation. Co(II) and Nickle(II) Nitrate ($Co(NO_3)_2{\cdot}6H_2O$ and $Ni(NO_3)_2{\cdot}6H_2O$) used for investigation were of high purity (min 99%) having trace metal contents far below their detection limits.

2.2. Characterization techniques

The analyses of the Co(II) and Ni(II) content were carried out using a Varian, AA200 model, atomic absorption spectrophotometer with acetylene/air flame in emission mode (l = 324.7 nm for Co(II) and l = 232.0 nm for nickle, slit width = 0.2 nm). The X-ray diffraction (XRD) analysis was done with a Philips PW 1800 diffractometer equipped with graphite secondary monochromator. Instrumental and measuring conditions were as follows: CuK_α radiation, 60 kV/40 mA, divergence and receiving slits of FINE, 0.020° 2θ step, 0.75 h, using a time per step of 0.500 s. XRD pattern was collected from 2.010° to 60.000° (2θ). The elemental composition of the natural bentonites was determined by the X-ray Fluorescence (XRF). All the analyses were performed with Oxford ED-2000 using Xpertease software. A Philips model XL30 scanning electron microscope (SEM) with energy dispersive atomic X-ray spectroscopy (EDAX) was used to take micrographs of the bentonites. Prior to the analysis, the sample was dispersed in ethanol using an ultrasonic bath for SEM/EDX characterizations. Subsequently, a drop of the dispersion was applied to a holey carbon grid. Brunauer–Emmett–Teller (BET) specific surface area and pore size distribution of original samples of Mesh No. 16 [ASTM E:11] of bentonites were determined using the Quantachrome NOVA 2000e series volumetric gas adsorption instrument, which is a USA automated gas adsorption system using nitrogen as the adsorptive. The determination is based on measuring the nitrogen adsorption. Experiment for adsorption isotherms was performed at 77.3 K and at the relative pressure up to $P/P_0 \sim 0.99$. Moisture and gases such as nitrogen and oxygen which were adsorbed on the solid surface or held in the open pores were removed under the reduced pressure at 100°C for 8 h before measuring the specific surface area and pore size distribution. The pore size distribution of studied samples was calculated from desorption isotherms using the Barett-Joyner-Halenda (BJH) method. Thermo gravimetric curves were recorded on a SATA 1500 (Scientific Rheometric) TGA-DSC working in air atmosphere. The specimens were prepared in crucibles and analyzed in a temperature ranging from room temperature to 1,100°C with nearly 10 mg of each sample with a heating rate (dT/dt) of 10°C/min in the air atmosphere. Derivative thermo gravimetric (DTG) analysis curves were analyzed by derivative weight loss and heat flow. The Fourier transform infrared (FTIR) spectra of the bentonites were recorded between 400 and 4,000 cm^{-1} using a KBr method with a Bruker, Vector 22 model, spectrophotometer.

2.3. Swelling property experiments

The pH of bentonite is a useful variable in determining the surface charge properties of bentonite, mobility of loosely tied ions in bentonite which can be replaced with Co^{2+} and Ni^{2+} and therefore the adsorption behavior toward Co^{2+} and Ni^{2+}. For the purpose of this test method, the air-dried bentonite samples were sieved through a Mesh No. 16 sieve (1 mm sieve

mesh openings). Eight grams of each sample was thoroughly stirred at least for 5 min in a beaker containing 100 mL distilled water. The pH was then measured by a pH meter of Lutron, YK-2001 CT model. When making measurements with the pH electrode, the electrode was placed into the partially settled suspension to mitigate the suspension effect and the mixtures were kept at an approximately room temperature (25°C). The pH meter was calibrated with buffers of pH 4.0 and 10.0.

Swelling tests were carried out on the basis of ASTM D 5890-02 [50]. The Swell Index of bentonites was obtained by gradually adding a 2-g sample in about 0.1-g increments to 90 mL of reagent water in a 100-mL graduated cylinder. After 2 h from the last increment addition, the hydrating bentonites column for trapped air or water separation was inspected. The Swell Index values corresponding to the volume of hydrated samples were recorded in millimeters after a minimum of a 16-h hydration period from the last increment addition.

Methylene blue chloride powder (from Merck) was used in this study for measuring the cation exchange capacity (CEC) of a bentonite according to the European standard (spot test). This procedure was followed step-by-step [51,52]: (a) preparing the methylene blue solution by mixing 1.0 g of dry powder with 200 mL of deionized water; (b) preparing the soil suspension by mixing 10 g of oven-dried soil with 30 mL of deionized water; (c) adding the methylene blue solution to the soil suspension in 0.5 mL increments; (d) mixing the soil suspension for 1 min for each addition of MB; (e) removing a small drop of the suspension and place it on Fisher brand filter paper; and (f) determining the specific surface area from the amount of MB required to reach the end point. When the unabsorbed methylene blue formed a permanent light blue halo around the soil aggregate spot, the "end point" has been reached (i.e. the MB has replaced cations in the double layer and has coated all the mineral surfaces). The CEC is calculated with Eqs. (1) or (2):

$$\text{CEC} = \text{MB added (mL)} \times \frac{\text{MB dry Wt (g)}}{319.87} \times \frac{1{,}000}{\text{Vol. of MB Solution}} \times \frac{100\text{ g}}{\text{Clay dry Wt (g)}} \quad \text{(m Eq/100 g)} \tag{1}$$

or

$$\text{CEC} = \frac{\text{MB added (mL) Wt (g)}}{\text{Vol. of MB Solution (mL)}} \times \frac{1{,}000}{31.987} \quad \text{(m Eq/100 g)} \tag{2}$$

Adding 0.5 mL methylene blue solution in each step is low for clays with high CEC like bentonite. Therefore, in this research, 20 mL of methylene blue solution was added in each step and the suspension was stirred for 40 min.

For granulometric (particle size distribution) analysis, 500 g of each bentonite sample was ground using a jar and ball mill for an hour and the samples were passed through a US Standard Sieve Mesh No. 16. Then, approximately 250 g of bentonite from each sample was dried [53] for 4 h at 110°C. Samples of approximately 100 g to the nearest 0.1 g (0.1 g precision) were weighed and sieved to different dry US Standard Sieve Mesh Numbers. The sieves were shaken until no further material passed through each sieve. The residue was transferred to a watch glass weighed to the nearest 0.01 g, and the glass plus residue was weighed to the nearest 0.01 g. The percentage was determined by the amount passing through the sieve from the Eq. (3) reporting to the nearest 1%.

$$\%\text{ by weight through sieve} = \frac{W_1 - (W_3 - W_2)}{W_1} \times 100 \tag{3}$$

Herein, W_1 is the sample weight, W_2 is the watch glass weight, and W_3 is the watch glass weight plus residue.

For Sediment Index (S.I.) measurements, 1 g of bentonite with a specific percent of moisture content (M) was weighed with a balance having +/− 0.001 g of precision. Bentonite was gradually poured into the 100-mL graduated cylinder containing 90 mL of distilled water, and the suspension was completely mixed with a magnetic stirrer for at least 5 min to have a homogeneous suspension. Then, 10 mL of a normal solution of NH_4Cl was poured there into as a dispersant, and the suspension was completely mixed again. After 72 h, the volume of sediment (V) was measured and the Sediment Index was calculated as follows using Eq. (4):

$$\text{S.I.} = \frac{V}{100 - M} \times 100 \tag{4}$$

Herein, S.I. is the Sediment Index, V is the sediment volume, and M is the moisture content.

2.4. Adsorption experiments

To study the adsorption process, the volume and shaking time were fixed at 25 mL, pre-determined contact times ranged 24 h (the effect of equilibrium

time on the separation of Co(II) and Ni(II) was eliminated using the 24-h shaking time), and the amount of the bentonite was 0.3 g, respectively. Batch experiments with 0.3-g clay particles were used to investigate the effect of the type of the bentonite on the adsorption process. All the experiments were carried out under the ambient conditions and pH 6.5. An incubator rotary shaker (GALLENKAMP model) was used for shaking the adsorption batches at a shaking speed of 250 rpm in 100-ml-polyethylene-capped bottles. All plastic bottle and glassware were rinsed with distilled water, followed by acetone wash and then dried. In all experiments, the solute–adsorbent mixture was centrifuged at 12,000 rpm for 15 min to separate the adsorbent from the liquid. The used centrifuge was a SiGMA Laboratory 92K15C model. The upper liquid was collected to determine the concentration of Co(II) and Ni(II).

The final Ni(II) and Co(II) concentration was determined using an atomic absorption spectrophotometer with an air–acetylene flame. Analytical calibration was along with aqueous standards 2, 5, 10, and 20 ppm of Co(II) and Ni(II). The working standards for calibration of atomic absorption spectrophotometer were prepared by diluting stock solution of 0.01 N (295 ppm). Fresh calibrations were made each time before the analysis.

To assess the effectiveness of metal uptake at each metal concentration, the distribution coefficient (K_d and the percentage of adsorption (removal efficiency) were calculated using the following equations:

$$K_d = \frac{C_0 - C_e}{C_e} \times \frac{V}{m} \quad (5)$$

$$\%\,\text{Adsorption} = \frac{C_0 - C_e}{C_0} \times 100 \quad (6)$$

where K_d is distribution (mL/g), C_0 and C_e (mg/L) are the initial and the final or equilibrium concentration (mg/L), V is the volume of the solution (mL), and m is the mass of bentonite in solution (g). All the adsorption experiments were carried out in duplicate, and the average is used all through in the text.

3. Results

3.1. Characterization techniques

Comparative XRD patterns of the original bentonite clays are shown in Fig. 2. In each diffractogram, for the considered band, there is a characteristic peak for montmorillonite (smectite) and the others are related to Quartz, Bassanite, Cristobalite, Feldspare, Halite, and Calcite. To easily identify them, the referring peaks are marked with letter "M" to montmorillonite, "B" to Bassanite, "Cr" to Cristobalite, "F" to Feldspare, "H" to Halite, and "Ca" to Calcite.

The XRD pattern of the natural clays (Fig. 2) showed characteristic d-spacing of 4.46, 2.54 and 1.49 Å. So, the samples are bentonites. The peak at 4.45 Å further implies the 2:1 montmorillonite. The XRD pattern also indicated quartz (4.24 Å) for all samples. Sample *A*2 XRD pattern indicated Bassanite (3.01 Å), Cristobalite (4.05 Å), and Feldspare, i.e.

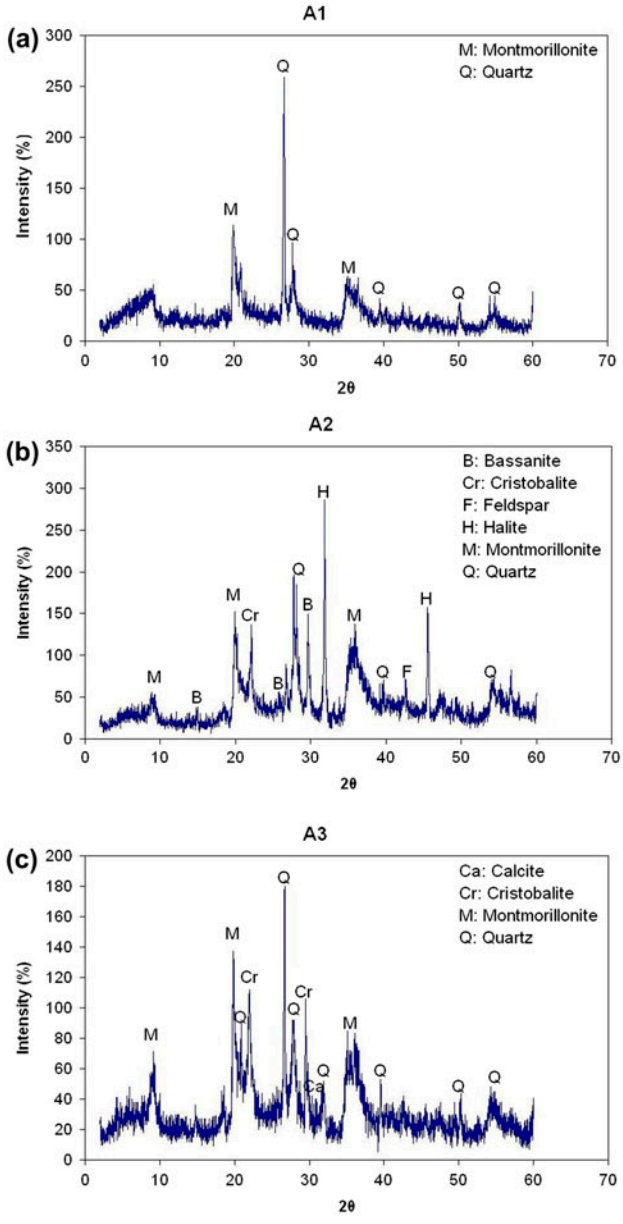

Fig. 2. XRD patterns of the original bentonite samples (a) *A*1 (b) *A*2, and (c) *A*3.

Albite, (2.12 Å) and Halite (2.82 Å). Sample *A*3 XRD pattern indicated Cristobalite (4.05 Å) and Calcite (3.03 Å). The natural bentonite clays have a d-spacing of 16.58, 15.17, and 17.35 Å, respectively [54]. The increase in d-spacing was because of the cation exchange and causes an expansion in the interlayer spacing. Subtraction of the thickness of the 2:1 layer of 9.60 Å yields an interlayer separation of 6.98, 5.57 and 7.75 Å in samples *A*1, *A*2, and *A*3, respectively.

SEM identifies the surface morphology and size of the montmorillonite. Montmorillonite which has a typical composition $Na_{0.33}Al_2$-$Si_4O_{10}(OH)_2{\cdot}nH_2O$ is flake-like crystals with fluffy and porous appearance revealing its extremely fine structure. Montmorillonite particles are heterogeneous and irregular with a ranging size between several μm to about 100 μm, with most particles measuring about 2–10 μm composing up to 16 montmorillonitic layers. Microstructure studies of bentonite samples (magnification 5,000×, 10,000× and 2,000×) reveal that there are so many micro-passages and even nano-passages in these samples (the black parts) in Fig. 3, some of these passages are open pores and some of them partially open pores; therefore, an aqueous solution like water containing Co(II) or Ni(II) will soak into these micro- and nano-tunnels. Each montmorillonite particle has an excess of negative charge in the lamellae generated by partial substitution of Al(III) by Mg(II) ions in the reticule. The negative surface helps to adsorb positively charged species such as Co(II) and Ni(II) ions through electrostatic interaction. The edge of the montmorillonite particle has few positive charges thus attracting negatively charged ions (like electrons). The white parts in Fig. 3 located at edges or needle-like parts are the result of attraction electron beams by positively edged charges.

EDX elemental analysis was performed at several different points of the surface in order to minimize any possible anomalies arising from the very pores of the analyzed surface (Fig. 3), but the elemental composition should be viewed as a rough estimation of the whole samples. This uncertainty is due to the limitations of the depth of the analysis, and the number of spots detected by EDX. Thus, the chemical compositions of the three bentonite samples are required.

The chemical compositions (XRF analysis) of bentonites are given in Table 3. The analyzed elements were in the form of percentage oxides as Na_2O, CaO, SiO_2, Al_2O_3, MgO, P_2O_5, SO_3^{2-}, Cl^-, K_2O, TiO_2, TFeO ($FeO+Fe_2O_3$), and H_2O.

Table 3 shows that the amount of CaO in sample *A*3 is high. A portion of the available CaO in sample *A*3 is attributed to calcite (XRD results of Fig. 2(c)). The largest amount of Al_2O_3 composing sample *A*1 indicates a higher amount of montmorillonite.

The values for the surface area by the BET single- and multi-point method along with pore diameter for clay samples are shown in Table 4, with typical nitrogen adsorption–desorption isotherms (Fig. 4). The nitrogen adsorption/desorption isotherms of the natural and modified bentonite are shown in Figs. 4 and 5. Apparently, their characteristic features, i.e. the hysteresis loops are associated with the capillary condensation in meso-pores. The surface area measurements by the BET method (Fig. 4) showed that *A*1, *A*2, and *A*3 had a pore distribution with a type II adsorption isotherm in the classification of Brunauer, Deming, Deming and Teller, characteristic of the multi-layered formation of adsorbed molecules on the solid surface, due to the presence of a meso-porous texture (in addition to the nano-porous) with large pores [55]. The rising final parts of the isotherms ($p/p_0 > 0.95$) in Fig. 4 also show the occurrence of macro-pores in the pore structures of studied samples [56].

The pore size distribution of studied samples is shown in Fig. 5. According to the classification of pores diameter size [57], the total porosity is classified into three categories according to the pore diameters. The categories are as follows: macro-pores ($d > 50$ nm), meso-pores ($2 < d < 50$ nm), and micro-pores ($d < 2$ nm).

In Fig. 5, there are micro- and meso-pores in all samples with predominant meso-porosity (Table 4). Showing in Fig. 4, the micro-pores (V_{mi}) and the meso-pores (V_{mes}) volumes are obtained through the reading of adsorbed volume (V_{ads}) in $P/P_0 = 0.10$ and 0.95 expressed by Eqs. (7) and (8) [58].

$$V_{mi} = V_{ads\,(P/P_0=0.10)} \tag{7}$$

$$V_{mes} = V_{ads\,(P/P_0=0.95)} - V_{ads\,(P/P_0=0.10)} \tag{8}$$

V_{mi} and V_{mes} calculation results are summarized in Table 5. The results show the surface area, meso- and micro-pore volume values are arranged in the following sequence: $A2 > A3 > A1$.

The thermo gravimetric (TG), DSC (TA), and DTG curves of samples *A*1, *A*2 and *A*3 are shown in Fig. 6. Bentonite has two major weight loss steps: 20–170°C, which correspond to loss of adsorbed water, and 450–800°C, which is caused by the loss of structure of the hydroxyl group. TG and DTG curves exhibit an initial dried weight loss of 7.1, 8.6, and 5.2% of initial mass for *A*1, *A*2, and *A*3, respectively, starting at 21°C and ending at 168°C. Major decomposition is started at 400°C with a weight loss of 18.2, 9.7, and 5.8% of initial mass for *A*1, *A*2, and *A*3, respectively.

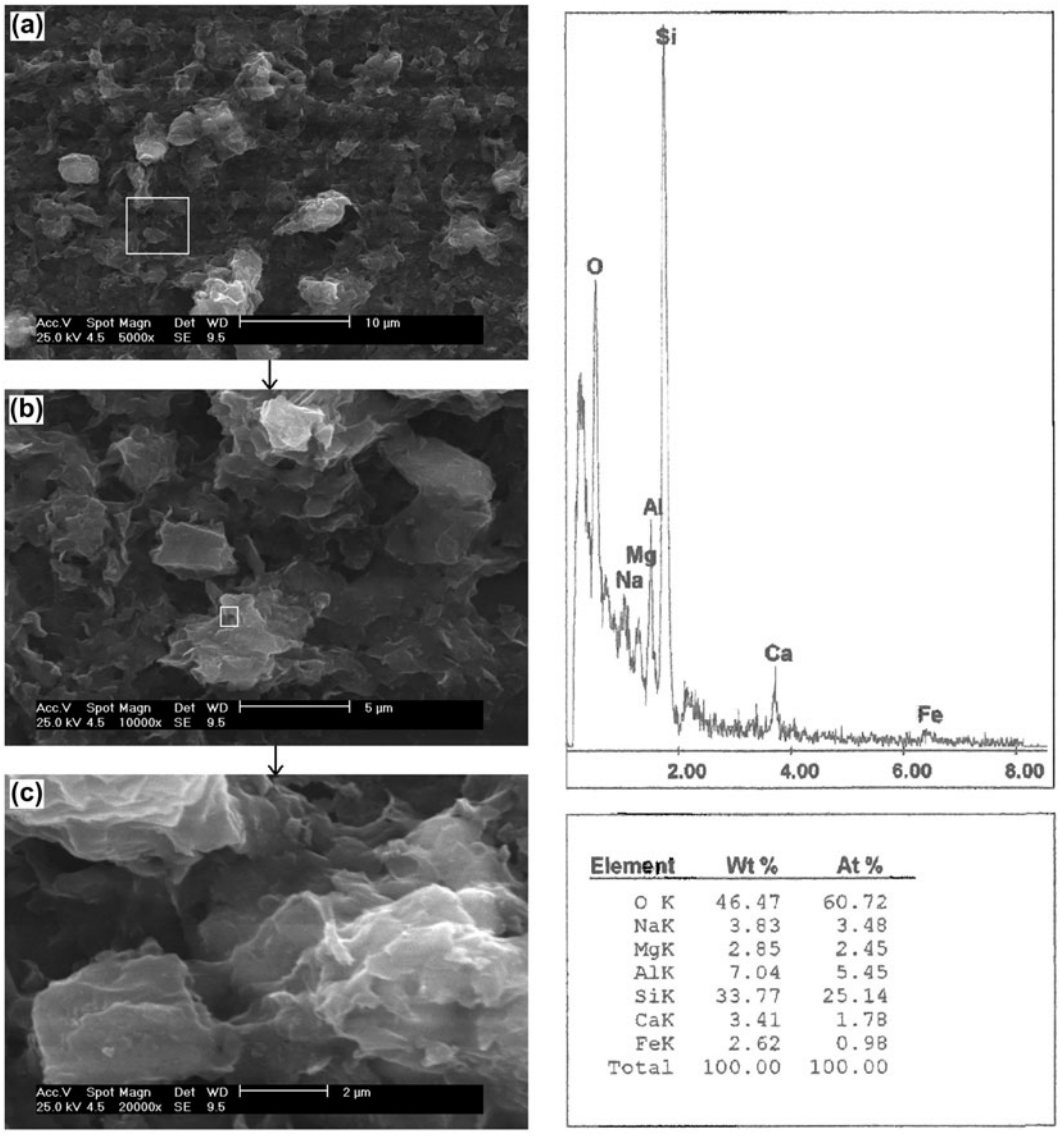

Fig. 3. SEM micrographs with EDX of sample *A*2 (a) 5,000×, (b) 10,000×, and (c) 20,000×.

Table 3
XRF results of studied bentonite samples

Analyte (wt%)	Na_2O	CaO	SiO_2	Al_2O_3	MgO	P_2O_5	SO_3	Cl	K_2O	TiO_2	TFeO[a]	H_2O
*A*1	1	0.2	71.6	22	2.2	0.7	–	–	0.1	–	1.8	1
*A*2	2.2	0.2	64.4	14.3	3.6	0.6	5.5	5.5	0.2	0.5	2	2.5
*A*3	2	2.9	71.6	13.2	2	0.3	0.3	0.2	0.4	0.5	3.6	2

[a]TFeO = FeO + Fe_2O_3.

FTIR values help identify the structure of bentonites. The FTIR spectra of samples *A*1, *A*2, and *A*3 are shown in Fig. 7, and the FTIR band assignments for samples compared with reference bands are reported in Table 6. The broad absorption bands observed in samples *A*1, *A*2, and *A*3 at 3,422 cm^{-1} represent the fundamental stretching vibrations of different –OH groups present in Mg–OH–Al, Al–OH–Al, and Fe–OH–Al units

Table 4
A_{BET} (single- and multi-point BET) and BJH method average pore diameter

Sample name	A_{BET} (m^2/g) single-point BET	A_{BET} (m^2/g) multi-point BET	Average nano-pore diameter (nm) BJH method
*A*1	14.4338	14.487	3.6104
*A*2	50.9885	50.979	2.8954
*A*3	17.3808	17.909	3.6763

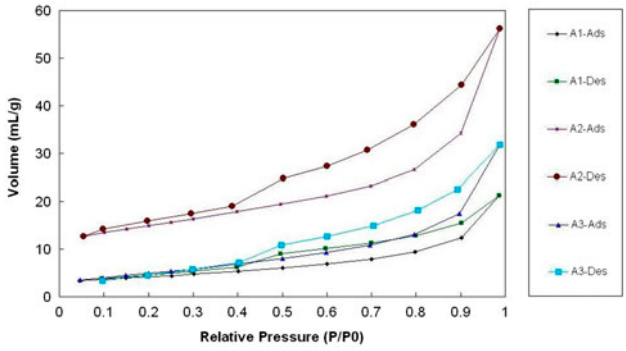

Fig. 4. N_2 adsorption/desorption isotherms of bentonite samples.

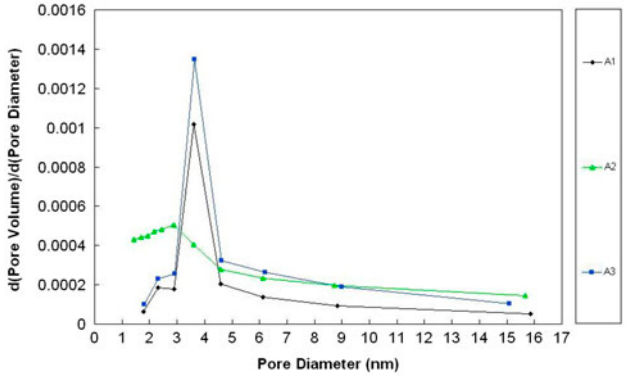

Fig. 5. Pore size distribution of studied bentonite samples.

in the octahedral layer [59]. It is shown that the peaks that correspond to the OH–stretching in spite of a small deviation in band positions remain the same for all samples. The presence of H_2O is confirmed by the adsorption at approximately 1,639 cm^{-1} corresponding to the H–O–H deformation. The bending mode of Al–OH–Al appeared at 917 cm^{-1}, whereas O–Si–O asymmetric stretching mode appeared at 1,035 cm^{-1}. The peak at 793 cm^{-1} (which shows existence of quartz) and weak band at 684 cm^{-1} were assigned to O–Si–O asymmetric stretching; the asymmetric bending mode of O–Si–O peak is at 457 cm^{-1} as reported in silicate system [60].

3.2. Swelling property experiments

Results of pH, Swell Index, Sediment Index, CEC of *A*1, *A*2, and *A*3 are listed in Table 7. The results of pH measurements followed the order of $A1 > A2 > A3$ being the same for Swell Index, Sediment Index, CEC values of *A*1, *A*2, and *A*3.

Table 8 indicates the content of finer parts of sample *A*1 (passing Mesh No. 400 or finer than 36 μm) is higher than that of the others, and the coarser parts are observed for sample *A*3 (finer than Mesh No. 16 (1,000 μm) but greater than Mesh No. 120 (125 μm)).

The swelling property experiment results also indicate swelling (Na-montmorillonite), nonswelling–swelling (Ca,Na-montmorillonite), and nonswelling (Ca-montmorillonite) type of bentonites for samples *A*1, *A*2, and *A*3, respectively.

3.3. Adsorption experiments

Table 9 shows the Co(II) and Ni(II) adsorption efficiencies along with their distribution coefficients achieved for bentonite samples *A*1, *A*2, and *A*3 for an

Table 5
V_{mi} and V_{mes} calculation results

Sample Name	$V_{ads\,(P/P_0=0.10)}$ (mL)	$V_{ads\,(P/P_0=0.95)}$ (mL)	$V_{mi.}$ (mL)	V_{mes} (mL)
*A*1	3.6847	17.5441	3.6847	13.8594
*A*2	13.4660	46.5784	13.4660	33.1124
*A*3	4.0089	25.7518	4.0089	21.7429

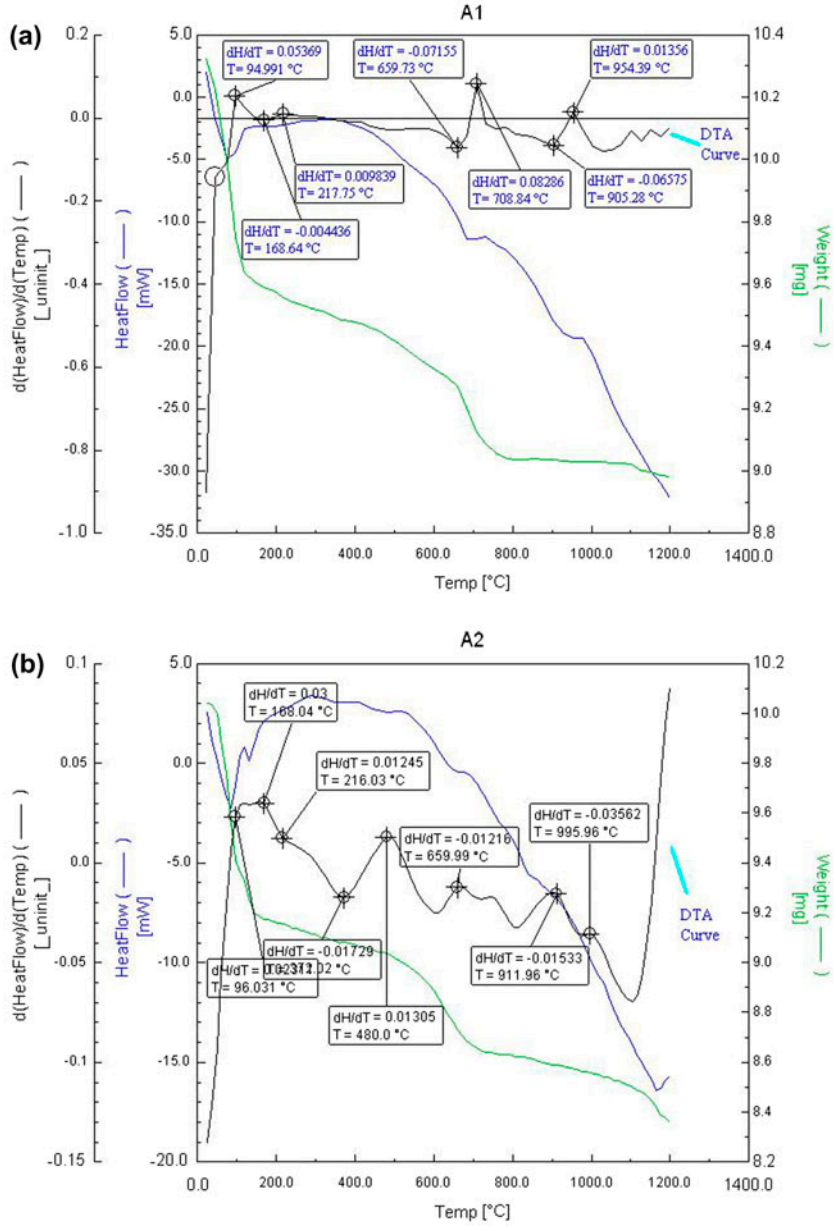

Fig. 6. The thermo gravimetric (TG), DSC (TA), and DTG curves of samples (a) *A*1, (b) *A*2, and (c) *A*3.

initial Co(II) and Ni(II) concentration of 0.01 N (295 mg/L) of their solutions. The other operation parameters were constants. The removal efficiency of both Co(II) and Ni(II) followed the order of *A*1 > *A*2 > *A*3 being the same for the distribution coefficient order.

The adsorption efficiencies and distribution coefficient for removal of Co(II) and Ni(II) are the same for sample A1 which is also the highest value (92% and 1,009 mL/g). The reason for not reaching the higher adsorption efficiency than that of 92% maximum adsorption efficiency is that as it nears equilibrium, the adsorbent surface becomes difficult to be filled in owing to the repulsive forces between the metal ions bound on the bentonites and the metal ions still present in the solution. The adsorption efficiencies decrease for Ni(II) comparing to Co(II) by 10 and 26% in sample *A*2 and *A*3, respectively.

It must be mentioned that chemical precipitation was minimal since the pH value was 6.5. The increase of pH to values greater than 7 resulted in significant increase of the Co(II) and Ni(II) ions that were

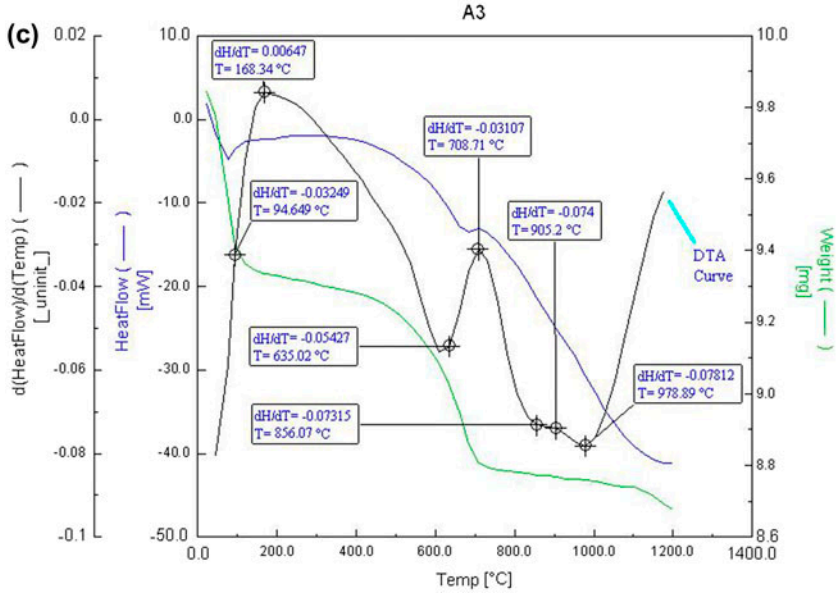

Fig. 6. (*Continued*)

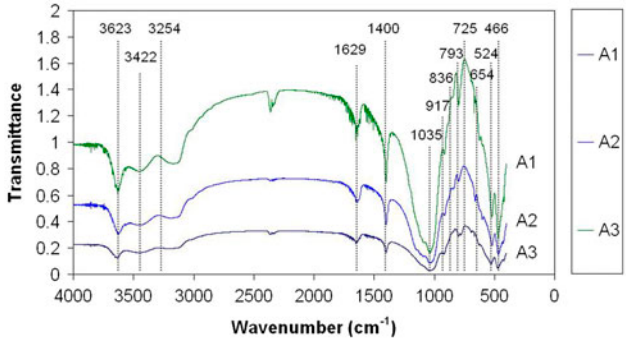

Fig. 7. FTIR spectra of samples *A*1, *A*2, and *A*3.

removed in bentonite, and this is associated with the initiation of chemical precipitation. A sharp increase in Ni(II) removal will be observed at pH > 7 for all minerals due to chemical precipitation in the form of hydroxides [61].

4. Discussion

EDX microanalysis confirmed the aluminic composition of montmorillonite of samples *A*1, *A*2, and *A*3. The spot EDX chemical analysis revealed a predominant composition of Si, Mg, and Al, with Fe, K, and Ca. The use of aluminosilicate adsorbents will be discussed in the following paragraphs as a feasible material for the removal of Co(II) and Ni(II) from aqueous solutions. Bentonite adsorption capacity depends not only on the metal type, but also on the type (swelling properties) of bentonite, as discussed here. The type of bentonite is directly defined by the result of bentonite characterization including pH, Swell Index, Sediment Index, CEC and granulometric (screen analysis) of bentonites (swelling properties experiments).

The comparatively high CEC and Swell Index values of the sample "*A*1" (swelling type) indicate that the minerals have a high amount of montmorillonite content. The high amount of montmorillonite (the fine portion of sample) results in high surface area which is an important factor in adsorption of Co(II) and Ni(II). However, the measured BET surface area of sample *A*2 is higher than that of sample *A*1 but sample *A*2 (nonswelling–swelling type) adsorption is less than that of sample *A*1. This reveals that isomorphic substitution is an important factor for sample *A*1 adsorption properties. The highest CEC value of 100 m Eq/100 g for *A*1 is in agreement with higher possibilities of isomorphic substitutions.

Swelling bentonites of *A*1 has more loosely tied mono- and divalent cations which are released to solution during pH measurements (measured pH 10). The higher weight loss observed in *A*1 confirms the presence of hydrated intercalated species (as indicated by high CEC, Swelling Index and pH for *A*1) which are loosely located in the interlayer regions.

Generally, the results indicate that there is a direct relationship between swelling properties results of samples and Co(II) and Ni(II) removal of a bentonite

Table 6
FTIR band assignments for samples *A*1, *A*2, and *A*3 comparing with reference bands assignments

Maxima (cm^{-1})	Assignments	*A*1	*A*2	*A*3
3,623	–OH Stretching	3,619	3,614	3,619
3,422	–OH Stretching, Hydration	3,425	3,426	3,425
3,254	–OH Viberational	3,264	3,260	3,275
1,639	–OH Bending, Hydration	1,630	1,624	1,630
1,430–1,382	CO_3 stretching of calcite	1,394	1,398	1,400
1,035	Si–O Stretching, in-plane	1,018	1,017	1,025
917	Al–Al–OH Bending	915	910	910
836	Al–Mg–OH Bending	–	841	841
793	Free Silica	804	809	813
730	Quartz	730	735	734
654	–OH Bending	–	645	–
524	Al–O–Si Bending	519	513	516
466	Si–O–Si Bending	459	457	461

Table 7
pH, Swell Index, Sediment Index, and CEC of studied bentonites

Sample name	pH	Swell Index (mm)	Sediment Index (mm)	CEC (m Eq/100 g)
*A*1	10	30	75	100
*A*2	8	24	35	95
*A*3	7.5	22	1	75

Table 8
The screen (granulometric) analysis of particles of studied bentonite samples

Mesh No. (μm)	−16 + 120 (−1,000 + 125)	−120 + 200 (−125 + 75)	−200 + 325 (−75 + 40)	−325 + 400 (−40 + 36)	−400 (−36)	Total weight (g)
*A*1 (g)	10.85	21.34	23.26	4.20	40.20	99.85
*A*2 (g)	7.00	29.53	23.17	10.11	29.32	99.13
*A*3 (g)	31.83	23.54	17.17	6.55	19.28	98.91

Table 9
Adsorption efficiency and distribution coefficient (K_d) of samples *A*1, *A*2, and *A*3 ($V = 25$ mL, $m = 0.3$ g, and $C_0 = 295$ mg/L in Eqs. (5) and (6))

	% Adsorption		K_d (mL/g)	
Sample name	Co(II)	Ni(II)	Co(II)	Ni(II)
*A*1	92	93	77	77.5
*A*2	72	62	60	52
*A*3	66	40	55	33

which means they are dominated by the type of samples *A*1, *A*2, and *A*3.

For the adsorption of Co(II) on bentonites, the equilibrium time of 24 h was found to be the optimal contact time while the two to three hours of equilibration time is reported for Ni(II) removal [36]. The pH of the aqueous solution is a variable that controls cationic adsorption onto clay surface due to the change of clay surface properties. Since this study aims studying of the type of bentonite on the Co(II) and Ni(II) adsorption, the pH is considered constant (pH 6.5).

The main reason for Co(II) ions removal is cation exchange and surface adsorption. The higher values of CEC of *A*1 and *A*2 (100 and 95 m Eq/100 g, respectively) indicate the removal of Co(II) by cation

exchange mechanism is more than that of the removal of Co(II) with A3 which has only 75 m Eq/100 g CEC. Studies showed that up to pH 8, Co ions exists mainly as Co(II) ions and at pH 10, $[Co(OH)]^+$ predominates [62–64]. Since present adsorption studies were carried out at pH 6.5, Co(II) ions were the main species in the solution that was exchanged or adsorbed on bentonite. The mainly existing divalent cations ($Co(II)^{2+}$) is displaced with two protons primarily from the edges (more accessible part) of bentonite particles for each metal cation adsorbed while one proton is exchanged for each of the monovalent $[Co(OH)]^+$ species adsorbed. So, the amount of Co(II) exchanged on bentonite followed the order of $A1 > A2 > A3$ which is in reverse order for $[Co(OH)]^+$ exchange due to decreasing measured pH for samples. The pH order of $A1 > A2 > A3$ also reveals the sample $A1$ has the highest capacity to exchange protons with Co(II).

Isomorphic substitution in clays is also the reason for negatively porous surface of bentonite clay. SEM study showed positively white parts (Fig. 3) located in edges or needle-like parts. The broken bonds at the edges or needle-like parts of the tetrahedral sheets require adsorbed cations for charge balance. The number of such bonds is high for smaller particle sizes of $A1$. The hydrolysable Co(II) ions form $CoOH^+$ interacts with the negative charge (theoretically calculated [7.8 (+4)] + [0.2 (+3)] + [3.4 (+3)] + [0.6 (+2)] + [20 (−2)] + [4 (−1)] = −0.8 charge/unit cell) on bentonite and bentonite adsorbs Co(II) ions in the sheets of hydroxyl groups and bentonite pores. The negatively charged surfaces provide adsorption sites for Co(II) ion:

$$(\equiv Si{-}O^-)_2 + Co^{2+} \rightleftarrows (\equiv Si{-}O^-)_2{-}Co \quad (9)$$

The above adsorption mechanism is mainly surface complexation [64]. This adsorption of Co(II) from solution occurs through outer-sphere complex formation via electrostatic interaction. Few amount of adsorption in the form of the first hydrolytic complex $CoOH^+$ and the surface groups of silica is as follows:

$$\equiv Si{-}O^- + CoOH^+ \rightleftarrows \equiv Si{-}O^- \cdots CoOH^+ \quad (10)$$

Once certain surface sites have been occupied, further adsorption occurs in association with ions previously adsorbed rather than at other sites on the oxide surface which results in stronger adsorption at high surface coverage and high Co(II) solution concentration (here the solution is 0.01 N of $Co(NO_3)_2{\cdot}6H_2O$ or 295 ppm of Co^{2+}) [65]. The end of adsorption process is accomplished with the formation of a monolayer of Co(II) ions on the outer surface of clay and intraparticle diffusion onto the inner surface of the adsorbent particles through the film after 24 h [42].

The adsorption of positively charged Co(II) onto the positively charged edges and needle-like parts of a bentonite at pH 6.5 is the direct evidence of formation of chemical bonds between the bentonite surface and Co(II).

In addition, there is a high possibility of formation of complexes in the metal solutions between the exchange cations and the released co-anions from samples, so that hydrogen also exchanges onto the samples, which would result in an apparent over-exchange.

Swelling sample $A1$ has the highest value of fine particles of montmorillonite (Table 8). The N_2 molecules could not reach its inner surfaces in the N_2 surface measurements. So, the BET surface of $A1$ is the lowest compared to the other samples but the Co(II) ions with 0.423 nm hydrated radius could penetrate into the pores. The average nano-pores diameter of $A1$ is greater than that of $A2$ but less than that of $A3$ and the accumulation of pores is the largest in $A1$ due to the highest value of finer particles measured by granulometric analysis. The average nano-pore diameter of $A1$ is the direct result of montmorillonite amounts. The montmorillonite is the adsorbent of Co(II) ions. The highest average nano-pore diameter of $A3$ is as a result of non-montmorillonite constituents which are not effective for Co(II) uptake. Consequently, the amount of Co(II) adsorbed by $A1$ is the highest value (Table 9).

Table 8 shows the strong influence of particle diameter on the amount of useful removal of Ni(II). Sample $A1$ has the highest amount of fine particles (40.20% less than Mesh No.400 or 36 μm). That is why $A1$ has the 92% adsorption efficiency or $K_d = 77$ mL/g (Table 9). Thus, particles with smaller diameter show a greater amount of useful removal. Another reason for Ni(II) removal is bentonite pores. $A1$ has some more open pores since it has more fine particles. Therefore, direct adsorption into the micro- and meso-pores took place.

Since the Co^{2+} and Ni^{2+} ions diffuse into the inner structure of the sample $A1$, the available pores for diffusion become lesser. Consequently, the free path of the metal ions in the pore decreases with time, and the metal ions may also be blocked, but surface area and lamellar cation exchange still plays an important role in Co^{2+} and Ni^{2+} removal.

Simultaneous study of the effect of bentonite type on the removal of Co(II) and Ni(II) shows in single-metal systems, Co(II) and Ni(II) adsorption capacity on $A1$ is the same for both metals. This is due to the

balance between the positive and negative parameters affecting the removal of Co(II) and Ni(II) which will be discussed in the following paragraph. *A*2 and *A*3 have the less adsorption capacity over Co(II). This is not influenced only by the electronegativity value of a metal ion, where the values are arranged in the order: Co(II) (1.88) < Ni(II) (1.91). The influence of electronegativity will be more sensible when the difference in electronegativity of metals is high. There is more attraction between these two ions when their electronegativity difference is large. Co(II) being the most electronegative results in its preferential adsorption to the hydroxyl (–OH). The oxygen of hydroxyl group has an available pair of electrons that can form coordinated covalent bonds with a metal cation. The oxygen atom in the hydroxyl group has a strong attraction to its electron lone pairs. Electronegativity has positive influence in the Co(II) comparing to the Ni(II) removal, but it is not the key parameter.

The relative abilities of the solute ion species to compete for surface sites of bentonite is governed by factors such as valence, ionic radius, pH, and the solution activities. Because the pH of the solution was kept constant at 6.5 and both Ni and Co are divalent cations, the selectivity (penetration ability which is defined as the ratio of valence to hydrated radius) depends entirely on the hydrated radii of the ions. With a radius of 4.04 Å, Ni is smaller than Co (radius = 4.23 Å). Ni is more effective in reacting with the clay particles of bentonite because of its smaller size but the pH value of 6.5 may have led to precipitation rather than adsorption of the Co^{2+}. A very small amount of magnetic Co^{2+} was observed in the filter paper. So, the adsorption percent and consequently the Co^{2+} K_d values of sample *A*2 and *A*3 are higher than that of Ni^{2+} K_d values.

Note that there are a number of possible compounds of Co at a given valence [66]. These compounds result from surface complex formation of the metal cations with a single-coordinated OH group on the edges of the surfaces of bentonites. Thus, a surface adsorption mechanism may dominate in the simple Co ion-exchange mechanism. The nature of these compounds rather than the quantity is of prime importance for the higher amount of Co^{2+} removal by adsorption process in sample *A*2 and *A*3.

Another reason why higher amount of Co^{2+} removal observed in sample *A*2 and *A*3 when the concentration of the cation in the reacting solution becomes larger than the CEC (comparing the Co solution concentration to the CEC values of *A*2 and *A*3), the adsorption of additional cations is promoted, owning to sorbate–sorbate forces [67]. These attractive forces exist owing to van der Waals forces, which promote contact.

5. Conclusions

The adsorption of Co(II) on bentonite using samples *A*1, *A*2, and *A*3 was shown to be type dependent. Based on the analytical and experimental data, the following conclusions may be drawn: (a) Adsorption studies were also performed using different bentonite types of swelling (*A*1), nonswelling–swelling (*A*2) and nonswelling (*A*3). The adsorption of Co^{2+} ions onto bentonite followed the order of: $A1 > A2 > A3$. The amount of Co(II) adsorbed decreased with an increase in nonswelling properties, indicating that the adsorption was more favorable at higher montmorillonite content. The same phenomenon was observed in the adsorption of Ni^{2+}. (b) The adsorption of Co(II) and Ni(II) ions is favored at sample *A*1 within the studied samples. The reason is the presence of montmorillonite which affects the adsorption of Co(II) and Ni(II) in sorbent–Co(II) and Ni(II) system. The qualitative amount of montmorillonite is measured by granulometric (screen) analysis. (c) The swelling property is an important factor for the adsorption of heavy metal ions on bentonite *A*1 which is a swelling (Na-type) bentonite. (d) The adsorption of Co(II) and Ni(II) on bentonite is mainly dominated by cation exchange and surface properties. SEM analysis may be a very useful method for the observation of surface morphology of montmorillonites. It is predicted a small portion of Co(II) may be removed by chemical precipitation at pH 6.5. So, the adsorption capacity is higher for Co(II) compared to Ni(II) for single systems using samples *A*2 and *A*3.

References

[1] C.L. Chen, D. Xu, X.L. Tan, X.K. Wang, Sorption behavior of Co(II) on γ-Al_2O_3 in the presence of humic acid, J. Radioanal. Nucl. Chem. 273 (2007) 227–233.
[2] Sh.M. Yu, A.P. Ren, Ch.L. Chen, Y.X. Chen, X. Wang, Effect of pH, ionic strength and fulvic acid on the sorption and desorption of cobalt to bentonite, Appl. Radiat. Isot. 64 (2006) 455–461.
[3] Sh.M. Yu, X. Li, A. Ren, D. Shao, Ch Chen, X. Wang, Sorption of Co(II) on γ-alumina in the presence and absence of fulvic acid, J. Radioanal. Nucl. Chem. 268 (2006) 387–392.
[4] D. Xu, D. Shao, C. Chen, A. Ren, X. Wang, Effect of pH and fulvic acid on sorption and complexation cobalt onto bare and FA bound MX-80 bentonite, Radiochim. Acta 94 (2006) 97–102.
[5] S. Szöke, G. Pátzay, L. Weiser, Cobalt(III) EDTA complex removal from aqueous alkaline borate solutions by nanofiltration, Desalination 175 (2005) 179–185.
[6] M.G.A. Vieira, A.F. Almeida Neto, M.L. Gimenes, M.G.C. da Silva, Removal of nickel on Bofe bentonite calcined clay in porous bed, J. Hazard. Mater. 176 (2010) 109–118.

[7] R.P. Beliles, in: F.W. Oehme (Ed.), Toxicity of Heavy Metals in the Environment, Part 2, Marcel Dekker, New York, NY, 1978, pp. 547–616.
[8] S. Mor, R. Khaiwal, A. de Visscher, R.P. Dahiya, A. Chandra, Municipal solid waste characterization and its assessment for potential methane generation at Gazipur landfill site, Delhi: A case study, Sci. Total Environ. 371 (2006) 1–10.
[9] C. Volzone, L.B. Garrido, Retention of chromium by modified Al–bentonite, Cerâmica 48 (2002) 153–156.
[10] V.P. Kudesia, Water Pollution, Pregatiprakashan Publications, Meerut, 1990.
[11] R. Han, L. Zou, X. Zhao, Y. Xu, F. Xu, Y. Li, Characterization and properties of iron oxide-coated zeolite as adsorbent for removal of copper(II) from solution in fixed bed column, Chem. Eng. J. 149 (2009) 123–131.
[12] E. Katsou, S. Malamis, K.J. Haralambous, Industrial wastewater pre-treatment for heavy metal reduction by employing a sorbent-assisted ultrafiltration system, Chemosphere 82 (2011) 557–564.
[13] M.A. Rocha, F.J. Anaissi, H.E. Toma, K. Araki, H. Winnischofer, Preparation and characterization of colloidal $Ni(OH)_2$/bentonite composites, Mater. Res. Bull. 44 (2009) 970–976.
[14] A.K. Bhattacharya, S.N. Mandal, S.K. Das, Adsorption of Zn(II) from aqueous solution by using different adsorbents, Chem. Eng. J. 123 (2006) 43–51.
[15] G. Cimino, R.M. Cappello, C. Caristi, G. Toscano, Characterization of carbons from olive cake by sorption of wastewater pollutants, Chemosphere 61 (2005) 947–955.
[16] S.H. Lin, R.S. Juang, Heavy metal removal from water by sorption using surfactant-modified montmorillonite, J. Hazard. Mater. 92 (2002) 315–326.
[17] G. Borbély, E. Nagy, Removal of zinc and nickel ions by complexationmembrane filtration process from industrial wastewater, Desalination 240 (2009) 218–226.
[18] R. Molinari, T. Poerio, P. Argurio, Selective separation of copper(II) and nickel(II) from aqueous media using the complexation-ultrafiltration process, Chemosphere 70 (2008) 341–348.
[19] I. Kabdasli, T. Arslan, T. Ólmez-Hanci, I. Arslan-Alaton, O. Tünay, Complexing agent and heavy metal removals from metal plating effluent by electrocoagulation with stainless steel electrodes, J. Hazard. Mater. 165 (2008) 838–845.
[20] D. Kalderis, E. Tsolaki, C. Antoniou, E. Diamadopoulos, Characterization and treatment of wastewater produced during the hydro-metallurgical extraction of germanium from fly ash, Desalination 230 (2008) 162–174.
[21] B. Merzouk, B. Gourich, A. Sekki, K. Madani, M. Chibane, Removal turbidity and separation of heavy metals using electrocoagulation-electroflotation technique. A case study, J. Hazard. Mater. 164 (2008) 215–222.
[22] K. Kabra, R. Chaudhary, R.L. Sawhney, Solar photocatalytic removal of metal ions from industrial wastewater, Environ. Prog. 27 (2008) 487–495.
[23] E. Chilyumova, J. Thöming, Nanofiltration of bivalent nickel cations—model parameter determination and process simulation, Desalination 224 (2008) 12–17.
[24] M. Al-Anber, Removal of high-level Fe^{3+} from aqueous solution using natural inorganic materials: Bentonite, (NB) and quartz (NQ), Desalination 250 (2010) 885–891.
[25] H. Omar, H. Arida, A. Daifullah, Adsorption of ^{60}Co radionuclides from aqueous solution by raw and modified bentonite, Appl. Clay Sci. 44 (2009) 21–26.
[26] S. Ertuğrul, N.O. San, G. Dönmez, Treatment of dye (Remazol Blue) and heavy metals using yeast cells with the purpose of managing polluted textile wastewaters, Ecol. Eng. 35 (2009) 128–134.
[27] H. Yin, B. He, H. Peng, J. Ye, F. Yang, N. Zhang, Removal of Cr(VI) and Ni(II) from aqueous solution by fused yeast: Study of cations release and biosorption mechanism, J. Hazard. Mater. 158 (2008) 568–576.
[28] M. Betancur, P.R. Bonelli, J.A. Velásquez, A.L. Cukierman, Potentiality of lignin from the Kraft pulping process for removal of trace nickel from wastewater: Effect of demineralisation, Bioresour. Technol. 100 (2009) 1130–1137.
[29] C.O. Ijagbemi, M.H. Baek, D.S. Kim, Montmorillonite surface properties and sorption characteristics for heavy metal removal from aqueous solutions, J. Hazard. Mater. 166 (2009) 538–546.
[30] G. Kocasoy, Z. Güvener, Efficiency of compost in the removal of heavy metals from the industrial wastewater, Environ. Geol. 57 (2009) 291–296.
[31] H. Genc-Fuhrman, P. Wu, Y. Zhou, A. Ledin, Removal of As, Cd, Cr, Cu, Ni and Zn from polluted water using an iron based sorbent, Desalination 226 (2008) 357–370.
[32] S. Sirianuntapiboon, O. Ungkaprasatcha, Removal of Pb^{2+} and Ni^{2+} by bio-sludge in sequencing batch reactor (SBR) and granular activated carbon-SBR (GACSBR) systems, Bioresour. Technol. 98 (2007) 2749–2757.
[33] S. Congeevaram, S. Dhanarani, J. Park, M. Dexilin, K. Thamaraiselvi, Biosorption of chromium and nickel by heavy metal resistant fungal and bacterial isolates, J. Hazard. Mater. 146 (2007) 270–277.
[34] M.A. Hanif, R. Nadeem, M.N. Zafar, K. Akhtar, H.N. Bhatti, Kinetic studies for Ni(II) biosorption from industrial wastewater by Cassia fistula (Golden Shower) biomass, J. Hazard. Mater. 145 (2007) 501–505.
[35] R.A. Axtell, S.P.K. Stenberg, C. Kathryn, Lead and nickel removal using microspora and lemna minor, Bioresour. Technol. 89 (2003) 41–48.
[36] K.G. Bhattacharyya, S.S. Gupta, Adsorption of a few heavy metals on natural and modified kaolinite and montmorillonite: A review, Adv. Colloid Interface Sci. 140 (2008) 1–55.
[37] J. Ayala, J.L. Vega, R. Alvarez, J. Loredo, Retention of heavy metal ions in bentonites from Grau Region (Northern Peru), Environ. Geol. 53 (2008) 1323–1330.
[38] S. Karahan, M. Yurdakoç, Y. Seki, K. Yurdakoç, Removal of boron from aqueous solution by clays and modified clays, J. Colloid Interface Sci. 293 (2006) 36–42.
[39] A.M. Fernández, B. Baeyens, M. Bradbury, P. Rivas, Analysis of the porewater chemical composition of a Spanish compacted bentonite used in an engineered barrier, Phys. Chem. Earth. 29 (2004) 105–118.

[40] F. Wypych, K.G. Satyanarayana, Clay Surfaces: Fundamentals and Applications, Elsevier Academic Press, London, 2004.
[41] D.M. Manohar, B.F. Noeline, T.S. Anirudhan, Adsorption performance of Al-pillared bentonite clay for the removal of cobalt(II) from aqueous phase, Appl. Clay Sci. 31 (2006) 194–206.
[42] X.L. Li, C.L. Chen, P.P. Chang, S.M. Yu, W.S. Wu, X.K. Wang, Comparative studies of cobalt sorption and desorption on bentonite, alumina and silica: Effect of pH and fulvic acid, Desalination 244 (2009) 283–292.
[43] N.M. Nagy, J. Kónya, Z. Urbin, The competitive exchange of hydrogen and cobalt ions on calcium montmorillonite, Colloids Surf., A. 121 (1997) 117–124.
[44] T. Shahwan, Ç. Üzüm, A.E. Eroğlu, I. Lieberwirth, Synthesis and characterization of bentonite/iron nanoparticles and their application as adsorbent of cobalt ions, Appl. Clay Sci. 47 (2010) 257–262.
[45] O. Abollino, M. Aceto, M. Malandrino, C. Sarzanini, E. Mentasti, Adsorption of heavy metals on Na-montmorillonite. Effect of pH and organic substances, Water Res. 37 (2003) 1619–1627.
[46] M. Shirvani, H.R. Rafiei, S. Bakhtiary, B. Azimzadeh, S. Amani, Equilibrium, kinetic, and thermodynamic studies on nickel removal from aqueous solutions using Ca-bentonite, Desalin. Water Treat. (2014) 1–9.
[47] E.F. Covelo, F.A. Vega, M.L. Andrade, Sorption and desorption of Cd, Cr, Cu, Ni, Pb and Zn by a fibric histosol and its organo-mineral fraction, J. Hazard. Mater. 159 (2008) 342–347.
[48] S. Malamis, E. Katsou, M. Stylianou, K.J. Haralambous, M. Loizidou, Copper removal from sludge permeate with ultrafiltration membranes using zeolite, bentonite and vermiculite as adsorbents, Water Sci. Technol. 61 (2010) 581–589.
[49] E. Álvarez-Ayuso, A. Garćia-Sánchez, Removal of heavy metals from waste waters by natural and Na-exchanged bentonites, Clays Clay Miner. 51 (2003) 475–480.
[50] ASTM D 5890-02, Standard Test Method for Swell Index of Clay Mineral Component of Geosynthetic Clay Liners, American Society for Testing and Materials, Pennsylvania, PA, 2002, pp. 1–7.
[51] J.C. Santamarina, K.A. Klein, Y.H. Wang, E. Prencke, Specific surface: Determination and relevance, Can. Geotech. J. 39 (2002) 233–241.
[52] Y. Yukselen, A. Kaya, Comparison of methods for determining specific surface area of soils, J. Geotech. Geoenviron. Eng. 132 (2006) 931–936.
[53] American Petroleum Institute (API), Spec 13A: Drilling Fluid Materials, Section 4: Bentonite, American Petroleum Institute, New York, NY, 1994.
[54] M. Hayati-Ashtiani, New insights to characterize mineralogical and physiochemical properties of nanoporous and nanostructured bentonites (Montmorillonites), Part. Sci. Technol. 30 (2012) 474–481.
[55] S. Brunauer, P.H. Emmett, E. Teller, Adsorption of gases in multimolecular layers, J. Am. Chem. Soc. 60 (1938) 309–319.
[56] K.S.W. Sing, D.H. Everett, R.A.W. Haul, L. Moscou, R.A. Pierotti, J. Rouquérol, T. Siemieniewska, Reporting physisorption data for gas/solid systems, Pure Appl. Chem. 57 (1985) 603–619.
[57] IUPAC, Physical Chemistry Division, Commission on Colloid and Surface Chemistry including Catalysis, Reporting physisorption data for gas/solid systems with special reference to the determination of surface area and porosity, Pure Appl. Chem. 57 (1985) 603–619.
[58] J.G. Gañán-Gómez, A.M. Macías-García, M.A.D. Díaz-Díez, C.G. González-García, E.S. Sabio-Rey, Preparation and characterization of activated carbons from impregnation pitch by $ZnCl_2$, Appl. Surf. Sci. 252 (2006) 5976–5979.
[59] V.C. Farmer, Infrared Spectra of Minerals, Mineralogical Society, London, 1974.
[60] H.V. Olphen, J.J. Fripiat, Data Handbook for Clay Minerals and Other Non-metallic Materials, Pergamon Press, London, 1979.
[61] Z.R. Liu, S.Q. Zhou, Adsorption of copper and nickel on Na-bentonite, Process Saf. Environ. Prot. 88 (2010) 62–66.
[62] S. Tsai, K. Juang, Y. Jan, Sorption of cesium on rocks using heterogeneity-based isotherm models, J. Radioanal. Nucl. Chem. 266 (2005) 101–105.
[63] T. Missana, M. Garcia-Gutierrez, U. Alonso, M. Mingarro, On radionuclide retention mechanism in fractured geological media, J. Iber. Geol. 32 (2006) 55–77.
[64] B. Baeyens, M.H. Bradbury, A mechanistic description of Ni and Zn sorption on Na-montmorillonite, part I: Titration and sorption measurements, J. Contam. Hydrol. 27 (1997) 199–222.
[65] K. Csobán, M. Párkányi-Berka, P. Joó, P. Behra, Sorption experiments of Cr(III) onto silica, Colloids Surf., A. 141 (1998) 347–364.
[66] S.A. Adeleye, R. Rautiu, D.A. White, Clay minerals as sorbents for nuclear reactor activation products, J. Mater. Sci. 30 (1995) 583–586.
[67] S.J. Gregg, K.S.W. Sing, Adsorption, Surface Area and Porosity, Academic Press Inc, London, 1982, pp. 5–49.